



Hyperspectral database of fruits and vegetables

ROBERT ENNIS, FLORIAN SCHILLER, MATTEO TOSCANI, AND KARL R. GEGENFURTNER*

Department of Psychology, Giessen University, Otto-Behaghel-Str. 10, 35394 Giessen, Germany

*Corresponding author: gegenfurtner@uni-giessen.de

Received 2 November 2017; revised 23 January 2018; accepted 9 February 2018; posted 9 February 2018 (Doc. ID 312492); published 14 March 2018

We have built a hyperspectral database of 42 fruits and vegetables. Both the outside (skin) and inside of the objects were imaged. We used a Specim VNIR HS-CL-30-V8E-OEM mirror-scanning hyperspectral camera and took pictures at a spatial resolution of ~ 57 px/deg by 800 pixels at a wavelength resolution of ~ 1.12 nm. A stable, broadband illuminant was used. Images and software are freely available on our webserver (<http://www.allpsych.uni-giessen.de/GHIFVD>; pronounced “gift”). We performed two kinds of analyses on these images. First, when comparing the insides and outsides of the objects, we observed that the insides were lighter than the skins, and that the hues of the insides and skins were significantly correlated (circular correlation = 0.638). Second, we compared the color distribution within each object to corresponding human color discrimination thresholds. We found a significant correlation (0.75) between the orientation of ellipses fit to the chromaticity distributions of our fruits and vegetables with the orientations of interpolated MacAdam discrimination ellipses. This indicates a close relationship between sensory processing and the characteristics of environmental objects. © 2018 Optical Society of America

OCIS codes: (330.1710) Color, measurement; (330.1720) Color vision; (100.2960) Image analysis.

<https://doi.org/10.1364/JOSAA.35.00B256>

1. INTRODUCTION

When preparing dinner, the choice of foods is at least partly determined by their color. Brown, moldy foods are likely to be discarded in favor of greener, more saturated, or more colorful foods. In addition, the color of foods can be indicative of whether they are poisonous or not [1]. Naturally, then, it is worthwhile to investigate the distribution of colors on foods, such as fruits and vegetables. While eating fruits and vegetables, we not only experience the colors of their skins, but also those on the inside of the fruits and vegetables. We made hyperspectral measurements of the colors of the skins and the insides of fruits and vegetables, and looked at the relationships between them. We made our hyperspectral measurements publicly available in Giessen’s Hyperspectral Images of Fruits and Vegetables Database (GHIFVD; pronounced “gift”). The database can be found at: <http://www.allpsych.uni-giessen.de/GHIFVD>. The properties of our measurements are described in this paper.

In the past, one possibility for measuring the colors on an object would have been to use a spectrophotometer and sample many points on the object’s surface. However, this process is error-prone, tedious, and of low spatial resolution. Another option would have been to use a calibrated RGB camera to evaluate the spectral response of each of its sensors. Information about the underlying spectra would have been gained by taking several photos of the object using different color filters [2,3].

However, this process can also be tedious, might require assembling the device or code, and, unless the camera is a well-designed industrial device, its measurements will be prone to noise and the camera might run various image processing algorithms that are designed to produce aesthetically pleasing images, instead of scientifically accurate ones. In recent time, hyperspectral cameras, which combine the spectral resolution of a spectrophotometer with the spatial resolution of a camera, have become a more prominent and accessible tool, although they are still very expensive. A hyperspectral camera will take an image like a regular camera, but each pixel will contain a recorded spectral distribution, rather than three RGB values. These cameras have advanced to the point that they rival dedicated spectrophotometers in their accuracy and precision, making them a prime choice for evaluating the distribution of colors on natural objects. Here, we have made use of a hyperspectral camera to build an image database of 42 fruits and vegetables, and we have evaluated the distribution of colors on their skins and insides.

Hyperspectral cameras have previously been used for the investigation of colors in natural scenes [4–7]. Using these images, a number of properties for colors in natural scenes have been documented. For example, Párraga *et al.* [7] analyzed the spatial frequency content of a set of hyperspectral images of natural scenes in terms of chromatic and luminance

information. Their results suggest that natural scenes contain a portion of high spatial frequency chromatic information, which is not captured by human vision. In fact, the human visual system is characterized by low-pass spatial filtering for chromatic signals, and bandpass filtering for luminance signals [8]. Hansen and Gegenfurtner [9], after analyzing the same set of images (in addition to a larger set of calibrated RGB images), proposed that chromatic edge contrast provides information for object segmentation which is to some extent independent of the information carried by luminance edges. Aside from this, metamers have been shown to be essentially nonexistent in natural scenes [10]. Metamers are two physically distinct stimuli that appear to be perceptually identical. The classical example is two surfaces that reflect different spectral distributions of light, but which appear to have identical colors to an observer. Metamers pose potential problems for color constancy, because one can potentially find two surfaces that are perceptually distinct under one illuminant, but are indistinguishable under another illuminant, rendering color constancy impossible for all possible situations. However, measurements of natural scenes found that the occurrence of metamers is very low, meaning that every distinguishable pair of surfaces should remain distinguishable under natural changes of the illumination. Hyperspectral imaging has also received interest from a computer vision perspective, and larger databases were made available and analyzed for different purposes, such as image reconstruction or face recognition [11–13].

For our database, we chose to narrow the scope from natural scenes down to the distribution of colors on the skins and insides of fruits and vegetables. The colors of the skins and the insides of fruits and vegetables are determined by the combined effects of a variety of colorants [14–16]. Investigations of the relationship between colorimetric measures and individual pigment concentrations are based on measures of the skins or the insides (for a review, see [16]), although the relationship between the chromatic properties of the skins and insides is not known. Here, we describe relationships between the colors on the skins and the insides of fruits and vegetables. More importantly, we demonstrate that once the colors on a fruit and vegetable have been represented in the Commission Internationale de l'Éclairage (CIE) xyY color space, the orientations of those distributions (as assessed by fitting ellipses) correlate well with the orientations of the MacAdam discrimination ellipses, which act as a measure of one's color discrimination capacities at different regions of color space [17]. We suggest that these findings imply: (a) the color of the skin of a fruit and vegetable could provide information about its inside and (b) our visual system is potentially tuned to discriminating the color distributions that are found in the natural environment.

2. METHODS

We have constructed a database of hyperspectral images consisting of both the insides and skins of 42 fruits and vegetables (see Table 1). The database serves as a cohesive set of images taken under controlled lighting conditions. In particular, we have made an attempt to provide a statistical summary of the colors in our data set, comparing them across the skins and insides of our fruits and vegetables. Lastly, we have compared the color distributions in our data set to known properties of color mechanisms in the human visual system.

A. Hyperspectral Camera

Our camera is a mirror-based scanning system with a CCD chip (VNIR HS-CL-30-V8E-OEM; Specim, Spectral Imaging, Ltd; Oulu, Finland). With standard settings, it records in 800 spectral bands, ranging from 376.20 nm to 821.62 nm, across 1600 spatial pixels. The spectral bands are not equally spaced in this camera, varying from 1.06 nm at the shorter wavelengths to 1.17 nm at the longer wavelengths, giving an average spacing of 1.12 nm. These spatial pixels are arranged in a line, such that only a single slice of a scene is recorded when one requests an image. A slice is also known as a frame, and the mirror-scanning system rotates to reflect different portions of a scene into the camera's optics, accruing frames that are eventually concatenated together to form a single image. As a result, the final image will be 1600 pixels high and its width will be dependent on the number of recorded frames. In addition, each pixel will contain 800 samples of the incoming spectrum, distributed across the visible range. In practice, we average the values of neighboring pixels and of neighboring wavelength bands to improve signal-to-noise ratio and to reduce the amount of time it takes to record a single image. This leaves us with a final image that is 800 pixels high and whose width is still dependent on the number of recorded frames, but where each pixel contains 400 spectral samples across the visible range. For the images in our database, the camera recorded at a frame rate of 8 Hz, giving an effective horizontal spatial resolution of ~57 px/deg. An example of how a hyperspectral image is decomposed into its constituent layers is shown in Fig. 1A. Lastly, please note that our camera only provides radiance measures for the light incident on its imaging sensor, and that is what we report and analyze in this paper. We made no attempt to estimate surface reflectance, since this is a difficult task for arbitrary three-dimensional objects, and our lab is not equipped for such measurements.

Our camera also contains adjustable optics. For our database, the lens was set to produce as focused an image as possible. This was ensured by placing a box with hard edges and written text at the center of the scene and making sure that the

Table 1. Fruits and Vegetables in Our Database

| | | | | | | |
|------------------|-----------------|-----------------|------------------|---------------|------------------|----------------|
| 1. Apple | 2. Artichoke | 3. Avocado | 4. Banana | 5. Blackberry | 6. Blueberry | 7. Carrot |
| 8. Cherimoya | 9. Coconut | 10. Cucumber | 11. Dragon fruit | 12. Eggplant | 13. Fig | 14. Grapefruit |
| 15. Green Pepper | 16. Green Apple | 17. Kiwi | 18. Kiwiberry | 19. Lemon | 20. Lime | 21. Mango |
| 22. Mushroom | 23. Nectarine | 24. Onion | 25. Orange | 26. Papaya | 27. Passionfruit | 28. Peach |
| 29. Pear | 30. Persimmon | 31. Plum | 32. Pomegranate | 33. Potato | 34. Pumpkin | 35. Radish |
| 36. Raspberry | 37. Red Cabbage | 38. Red Currant | 39. Red Pepper | 40. Red Chili | 41. Tomato | 42. Zucchini |

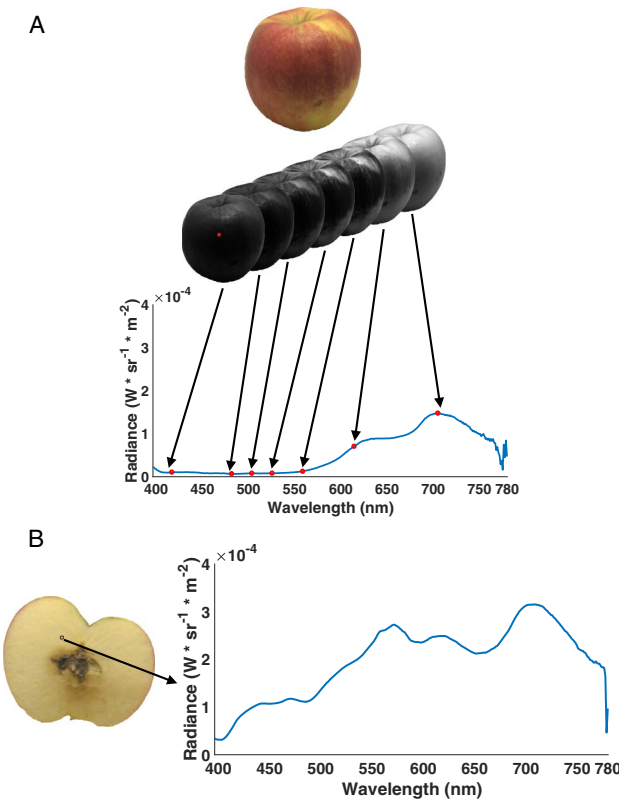


Fig. 1. Example of hyperspectral images and the layers that correspond to different measured wavelengths. A: The apple at the top was measured, producing a hyperspectral image that can be represented as several false color heat map images (middle row) that depict the intensity in the given wavelength band at each pixel. In the heat map, blacker marks less energy and whiter marks more energy. Each image in the middle row shows the incident radiance at the camera sensor for a specific wavelength band. The different images each indicate the spatial distribution for the chosen wavelength band, pointed to by the arrows and indicated by the red circles. We have only shown seven wavelength bands for visibility purposes; the complete hyperspectral image contains 368 bands. One can also concentrate on a single pixel, rather than a single wavelength band, as shown in the bottom row. The reflected spectrum measured for a pixel at the center of the image, indicated by red square on the first heat map, is shown. B: Sample spectrum for a pixel taken from the inside of the same apple. It shows that the inside is more reflective.

text was legible and that the edges produced a crisp change in response across the imaging sensor. Unfortunately, our camera does not have a very deep depth of field, since it is designed for use on airplanes that perform geological surveys, so one reaches a limit on how well the camera can be focused. At an imaging distance of 1 m, one can therefore notice significant drops in the focusing power after approximately 10 cm, either in front of or behind the point of focus.

B. Lighting System, Fruits, and Vegetables

We imaged the skins and insides of 42 different vegetables and fruits under a daylight-like illuminant. All of the fruits and vegetables were purchased from Rewe (Cologne, Germany), a

German supermarket. We purchased organic produce, when possible, to reduce the effects of waxes or genetic alterations that aim to enhance the skin color of a fruit and vegetable. See Fig. 2 for images of the fruits and vegetables in our database and see Figs. 1A and 1B for comparisons of example spectral measurements on the skin and inside of an apple. Please note that the red cabbage was too large to easily fit into the imaging box and make a complete image of it. Otherwise, we would have been required to move the camera, so we felt it best to keep imaging conditions constant, rather than giving one object preference over the others.

The illuminant was produced by a Thorlabs OSL2 stabilized light source (Thorlabs, Inc.; Newton, New Jersey, U.S.), that was filtered via a Thorlabs FGT05165 color-balancing filter to

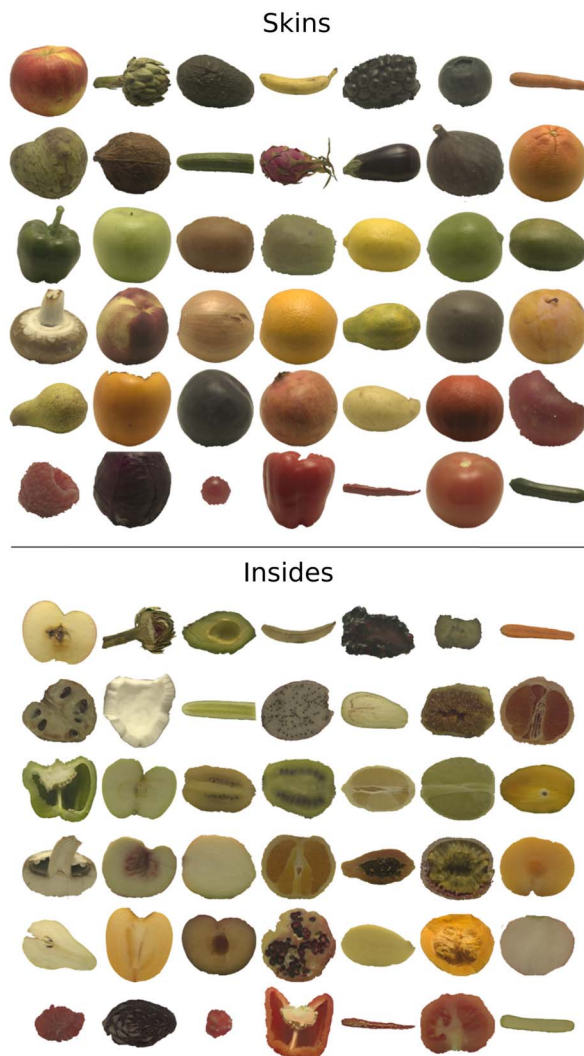


Fig. 2. Forty-two fruits and vegetables in our image database. The top panel shows the skins of each item and the bottom panel shows the corresponding insides. The list of all objects can be found in Table 1, where the items in this figure are listed from left to right, top to bottom. Please note that for the images shown in this paper, the RGB values have been increased for visibility purposes. Also, the image for the skin of the red cabbage is clipped at the top because it was too large for our imaging setup. See text for further details.

reduce the dominance of emitted long-wavelength light. The color-balancing filter had an effective conversion value of -160 mireds, giving the resulting illumination a correlated color temperature of 5506 K. The intensity of the light was always at its maximum. The CIE1931 xyY coordinates of the daylight-like illuminant were measured with a PR650 RS3 PTFE white reflectance standard (Photo Research, Inc.; Syracuse, New York, U.S.), placed at approximately a 45° angle, and a Konica CS-2000A spectrophotometer (Konica-Minolta, Inc.; Tokyo, Japan), which was placed at the same position, height, and pose as the hyperspectral camera was placed during the development of the database. The CIE1931 xyY coordinates of the daylight-like illuminant were [0.3324, 0.3435, 36.97 cd/m²].

The light was positioned approximately 11.5 cm above a white box with an open top. The front of the box was also open. The dimensions of the box were 25 cm × 25 cm × 27.3 cm. The light pointed directly downwards to illuminate the box. The walls of the box were provided by OBI GmbH (Wermelskirchen, Germany; German hardware supplier; article number: 4561528), who had prepainted them with a white paint that appeared mostly matte, with a slight hint of evenly applied gloss. This was the most matte prepainted wood available at our local store. We confirmed via spectral measurements with the Konica CS-2000A, a PR650 white reference, and a JUST Normlicht LED box (JUST Normlicht, GmbH; Weilheim, Germany), which has adjustable UV LEDs, that the white paint did not contain a fluorescent compound (i.e., the presence of UV light did not cause the measured spectral reflectance to become artificially increased in the visible range), even though the Thorlabs illuminator emits relatively weakly in the near UV range (average intensity relative to maximum = 0.022% from 300 to 400 nm, according to an online data sheet from Thorlabs, Inc.). The spectral reflectance of the paint, computed from a sample for each wall of the box, is shown in Fig. 3, as measured by a Konica CM-700d (Konica-Minolta, Inc.; Tokyo, Japan). To test the reliability of the manufacturing process, the same piece of wood was purchased from the same OBI storefront after two years, and it was essentially identical in spectral reflectance to that used for the box (RMSE = 0.0059%; see black dashed line in Fig. 3).

In order to reduce specular highlights and try to provide a more uniform illumination, we placed a layer of diffusive photographers' paper (Walimex Pro Diffusor; Walser, GmbH; Burgheim, Germany) across the opening at the top of the imaging box. Table 1 contains a list of the fruits and vegetables that we imaged. In all cases, the inside and the outside of each was imaged. When imaging the internals of our objects, we took care to cut them along an axis that would show as much of the inside as possible, while preserving a view of their typically symmetrical contents. We made attempts to lay each cut fruit or vegetable in a position that would prevent including the skin in an image. This was not always possible, and those images were segmented to remove the skin. Care was taken to clean up any juices from the cut fruits or vegetables. All images were taken at a distance of 48 cm, with the frontal plane of the hyperspectral camera placed at roughly 45° with the floor.

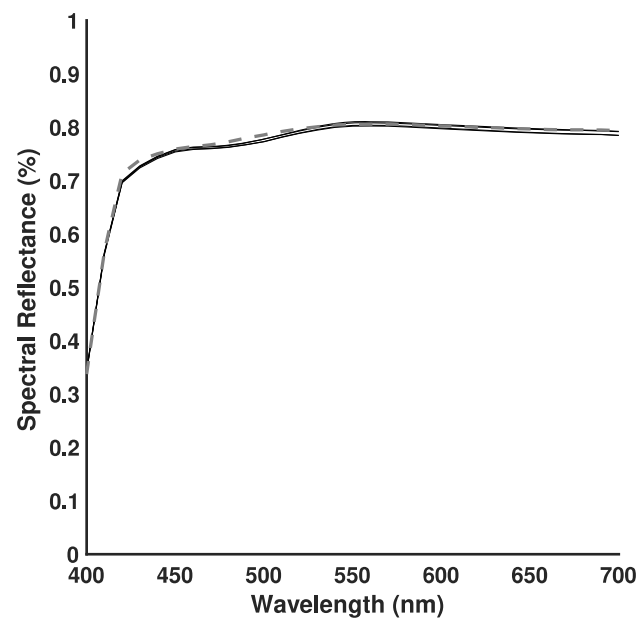


Fig. 3. Average spectral reflectance for the walls of our white imaging box, as measured with a Konica CM-700d, which samples from 400 nm to 700 nm in 10 nm steps. One sample was taken for each of the four walls. Each is shown as a thin black line to illustrate the high degree of overlap. The gray dashed line shows the measured reflectance of the same product, purchased two years later. The reflectance and its reproducibility is suitable for spectral measurements.

C. Image Processing

We wrote tools in the MATLAB (Mathworks, Inc., Natick, Massachusetts, U.S.; v2014b), C, and Rust v1.21.0 [18,19] programming languages for taking the raw data of the camera and converting that to calibrated radiance units. This is necessary, since the raw data of the camera are in binary units and do not have a direct physical meaning. They must be converted to physical units of energy using the calibration data provided by Specim. The C program made use of the OpenBLAS [20,21] linear algebra library and the libvips [22] multichannel image-processing library. The Rust program made use of the csv (v0.15.0), byteorder (v1.1.0), nalgebra (v0.13.1), num-traits (v0.1.40), and lodepng (v2.0.0) crates (i.e., Rust libraries) available on crates.io. The outputs of each program, as well as parts of their subroutines, were checked against each other, to be sure that each gave the correct values. Information was provided by Specim, Spectral Imaging, Ltd (Oulu, Finland) about how to properly process the data from their camera.

The final output of the programs consists of a calibrated hyperspectral image, where each pixel contains a spectrum in units of radiance ($\text{W} * \text{sr}^{-1} * \text{m}^{-2}$), as well as a representation of that image in the CIE1931 XYZ color space, ready for various color-processing operations. In addition, the programs provide a linear RGB image, specifically converted for the primaries of one of our experimental monitors (Sony OLED PVM2541-A; Sony, Corp.; Tokyo, Japan), and a gamma-corrected version of the linear RGB image, again converted

for the same experimental monitor, both meant for presentation purposes. For the images available in our database, this calibration and conversion process was carried out with the Rust program on Ubuntu Linux 16.04.3 LTS.

D. Database Interface

The MATLAB functions were supplemented by a MATLAB-based interface for querying, investigating, and segmenting a hyperspectral image. Image segmentation was greatly assisted by an OpenCV-based Python utility [23] that was written to make use of the GraphCut segmentation algorithm via the GrabCut implementation [24]. Our MATLAB-based interface allows a user to select either individual pixels or a rectangular subregion of an image in order to view the spectra at these locations, as well as their conversion to various color spaces of interest, including the CIELAB [25], CIELUV [25], MB-DKL [26,27], CIEXYZ/CIExyY [25], and LMS [28,29] color spaces. Lastly, if desired, the interface allows one to save statistics about either the whole image or selected subregions. These statistics are mainly first- and second-order moments along the cardinal axes of the different color spaces.

E. Image Compression and Noise Removal

We used MATLAB's *pca()* function (MathWorks Inc.; Natick, Massachusetts, U.S.; v2014b) in a program that extracts the first 10 principal components from an image for the purpose of image compression. This program can use those 10 principal components to reconstruct the original hyperspectral image, thereby rejecting the remaining principal components, which are typically noise. Similarly, Skauli and Farrell [11] have used a singular value decomposition (SVD) dimensionality reduction method to compress their images. SVD forms the core of a principal component analysis, and their approach allowed them to reduce file sizes for images of faces, landscapes, and buildings by at least a factor of 10, while preserving 99.99% of the variance for each hyperspectral image. A separate study [30] of principal component compression of hyperspectral images has shown that with the first seven principal components, one can produce an RGB image that is psychophysically indistinguishable from the original. However, we took the first 10 because our goal was to represent the full spectral data. For our hyperspectral images, the first 10 principal components accounted for $98.12 + - 0.82\%$ of the variance on average. The remaining components were essentially noise and removing them cleared up the signal, especially for spectral bands that did not contain much power. As a side effect, by saving only the first 10 principal components to a file, we saw up to a 75% reduction in file size, which is helpful, since for our setup, a single hyperspectral image can often be on the order of 700 MB–1 GB. We reduced file sizes even further by cropping the images and only saving the data for the fruits and vegetables after they had been segmented from the full image, since the full image also contained the imaging stage, which was not of interest in our analyses. When segmenting the images of the insides, we made sure to also segment any parts of the skin from the final images to prevent it from biasing our analyses. In addition to this, for the compressed images, we also discarded wavelengths below 396.40 nm, since those were typically noisy

for our system, as well as wavelengths above 779.61 nm, since the human visual system shows essentially no response above this value. The analyses described throughout the rest of this paper were performed with the values coming from this compression and noise-removal procedure.

F. Analysis of the Color Relationships between the Skins and the Insides

One goal of our study was to examine if there are regularities between the insides and the outsides of our fruit objects, as far as lightness, saturation, and hue are concerned. CIELAB space [31] allows for a representation of our fruit and vegetable objects in terms of lightness, saturation, and hue. In CIELAB, lightness is given by L^* and saturation can be defined as the distance of a color from the white point (which is also referred to as "chroma" and defined as $C^* = \sqrt{(a^*)^2 + (b^*)^2}$) divided by its lightness. Note that the CIELAB saturation measure agrees particularly well with human perception in the greenish, reddish, and yellowish color directions [32,33]. Since most of our objects have greenish, reddish, or yellowish colors, the CIELAB measure therefore is particularly suitable for quantifying the saturation of our objects. Hue is given by the angle between the abscissa and the line that connects (in the plane of equal lightness) the color, whose hue is to be determined, with the white point.

A fair comparison between the skins and the insides of the objects needs to take into account that there are differences in surface geometry of the objects and in the way they were placed in the imaging box. We attempted to cut and position the objects such that the surface along which the object was cut was perpendicular to the bottom of the imaging box [Fig. 4A]. The camera, however, was positioned such that more of the top part than of the bottom part of the intact objects was photographed. Thus, computing the mean lightness across the whole intact objects, whose upper surfaces were typically

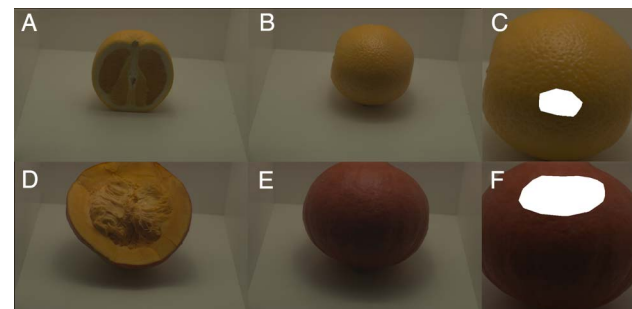


Fig. 4. A: Surface of the cut object is perpendicular to the bottom of the imaging box. We attempted to position the cut objects like this whenever possible. B: Intact object in imaging box. C: Closeup of the intact object shown in B. Marked in white is the surface area that was judged as having approximately the same orientation as the surface of the corresponding cut object in A. D: Object that could not be positioned such that the cut surface is perpendicular to the bottom of the imaging box. E: Intact object in imaging box. F: Closeup of the intact object shown in E. Area of the surface of the intact object that is comparable with the orientation of the surface of the cut object is marked in white. Note that this area is further on the top of the object than in C, since the surface of the cut object in D is tilted almost 45°.

oriented to reflect more light into the camera, would overestimate their lightness relative to that of their insides. However, in some cases, the mean lightness of the cut object might be overestimated, since it was not always possible to cut and position the object such that the cut surface was perpendicular to the bottom of the imaging box [Fig. 4D]. We tried to take into account the difference in geometry between intact and cut objects by considering only those parts on the surface of the intact object in our comparisons that had approximately the same orientation as the surface of the corresponding cut object [Figs. 4C and 4F]. That is, we computed the mean lightness value across the whole inside and compared this value to the mean lightness value that pertained to the area of the skin whose orientation was comparable.

To compare the saturation and hue of the insides and the skins, we had to determine a chroma value and hue angle for each object. In the case of the insides, we averaged the a^* and b^* values across the whole object and then determined chroma and the hue angle from these mean values. To obtain a value for saturation, we divided the chroma value by the mean lightness value that was computed from averaging across the whole cut object. In the case of the skins, we averaged a^* and b^* only across the area of the object that was comparable in its orientation to the orientation of the corresponding inside. Chroma and hue angle were then computed for this area only. To obtain saturation, we divided the value for chroma by the geometry-corrected lightness value.

G. Finding the Orientation of the Fruit Distributions

Each of the color distributions in our fruit and vegetable images form clouds in the CIE1931 xyY chromaticity diagram. For such two-dimensional point cloud distributions, a useful summary can be an ellipse that is fit to the distribution. There is already precedence for doing so in other reports of hyperspectral measurements [5,34,35]. Prior to fitting the ellipses, images were adjusted to exclude the stem if it was judged by eye to be of a different color from the skin on the fruit and vegetable. This was done for the persimmon, the red chili, the red pepper, and the radish. The distributions for each fruit and vegetable, as represented in the CIE1931 xyY color space, were preprocessed to remove noise. The distributions were first converted to the CIE1931 XYZ color space, and dark pixels were removed by excluding those where the sum of X, Y, and Z was less than 0.001 or where the Y component was less than 5% of the median Y value. Next, we used the exclusion criteria of [5]: the remaining points in the distribution were represented in the CIELAB color space and were projected into the isoluminant (a^* , b^*) plane. A two-dimensional histogram centered on the origin of the (a^* , b^*) plane with bin widths of 1 unit was computed, and those pixels in bins that had 10 or fewer points were also excluded from the analysis [5]. Last, the remaining pixels were represented in the CIE1931 xyY chromaticity diagram, and an ellipse was fit to the distribution using the eigenvectors of the covariance matrix as the major and minor axes, scaling them up to the 95% confidence interval. The orientations of the fitted fruit ellipses were then compared with the MacAdam ellipses [17], as discussed in more detail under “Color Distributions on the Skins of Fruits and Vegetables and Chromatic Discrimination” in the “Results.”

Note that of the 42 fruits and vegetables that we measured, only two had close to circular fits: the nectarine and the pear. Ellipses were the norm.

3. RESULTS

A. Color Relationships between the Skins and Outsides

It is not immediately clear how far the color on the skin of a fruit or vegetable can be used to predict the color of the inside, since the processes that regulate fruit formation vary substantially between plants [36]. Indeed, there are instances in which one may be surprised, as shown in Fig. 5. The eggplant in Fig. 5A may be familiar to many, and the color of its inside [Fig. 5D] may be expected, but if one has not seen a papaya before [Fig. 5B], then one may be unsure if its inside should really have the color seen in Fig. 5E. In addition, many people are puzzled when seeing the inside of a dragon fruit for the first time, which can be seen in Figs. 5C and 5F. This suggests that there are at least some unexpected relationships between the color of the skin on a fruit or vegetable and the color of the inside. So, are there regularities between the insides and the outsides of our fruit objects in lightness, saturation, and hue? This is the question we will examine in the following.

Using our analysis that corrects for the difference in geometry between the cut and the intact object, we found the mean lightness (45.56; range = [17.24; 75.80]) of the insides to be higher than the mean lightness (33.80; range = [10.32; 59.72]) of the skins ($t(41) = -6.032, p < 0.001$). This result is illustrated in Fig. 6A. This difference is still significant if the average lightness across the whole skin is used for the computations instead of the area of the skin whose geometry is comparable to that of the inside ($t(41) = -2.574, p = 0.014$). The correlation between the geometry-corrected lightness of the skins

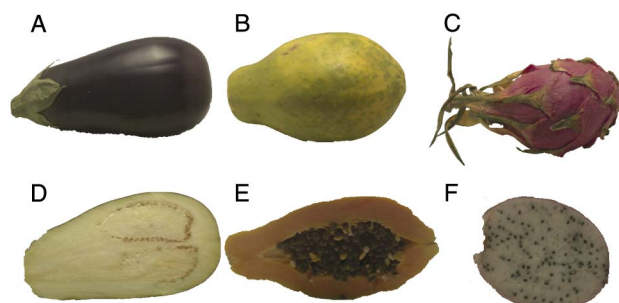


Fig. 5. Examples of potentially predictable and unpredictable foods. For those that are familiar with the eggplant A, they will probably expect its inside to look like the image in D. Similarly, those that are familiar with the papaya in B will probably expect it to be a bit redder with seeds on the inside, as visualized in E. In both cases, those who are unfamiliar with either the eggplant or the papaya might be a bit surprised about the insides. In the extreme case, as shown in C, a dragon fruit’s bright pink color probably does not lead to the initial expectation of a white inside with black seeds, as shown in F. Indeed, some who see the inside of a dragon fruit for the first time ask if it is edible and even how one should eat it (personal experience of the authors). These examples show that it is unclear whether the relationship between the outsides and the insides follows certain regularities. Hence, it is worthwhile to investigate whether such regularities exist.

and the insides was also significantly different from zero [$r = 0.461$, $t(40) = 3.289$, $p = 0.002$; see Fig. 6B].

Even though the insides were slightly less saturated than the geometrically matched areas of the outsides, this difference [Fig. 7A] did not reach significance ($t(41) = 1.848$, $p = 0.0719$). The correlation between the mean saturation of the objects' skins and their insides was significantly different from zero [$r = 0.406$, $t(40) = 2.812$, $p < 0.008$; see Fig. 7C]. We used the Jammalamadaka–Sarma circular correlation coefficient [37,38], as provided by the Circular Statistics toolbox for MATLAB [39], to examine the relationship between the hues of the insides and the geometrically matched areas of

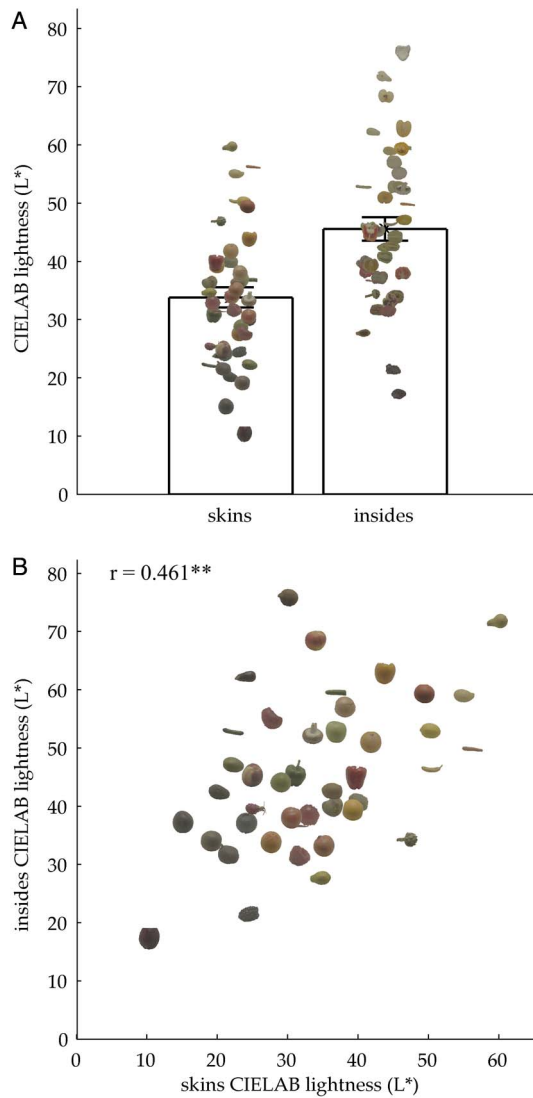


Fig. 6. Data points are depicted as small cutouts of the images of each fruit and vegetable. A: Bars represent average lightness of the insides of our fruits and vegetables and the geometrically matched areas of the outsides, as represented in the CIELAB space (L^* scale). Error bars represent the standard error of the mean. We find that the mean lightness of the insides is significantly higher than the mean lightness of the geometrically matched area of the skins. B: The lightness of the insides significantly correlates with the lightness of the geometrically matched areas of the skins, as indicated by the stars above the Pearson correlation value at the top of the graph.

the outsides of our objects. We found a significant circular correlation ($r_{\text{circular}} = 0.638$, $z = 3.495$, $p < 0.001$). These results are illustrated in Fig. 7B.

The above results can be summarized as follows: (1) lightness is, on average, higher on the inside of a fruit and vegetable than

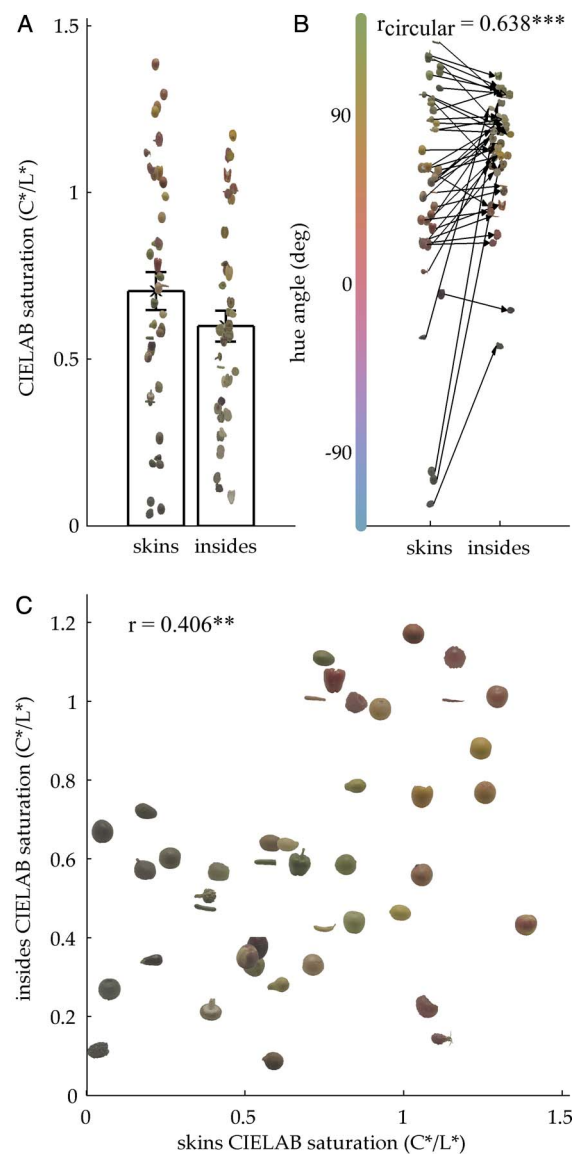


Fig. 7. Data points are depicted as small cutouts of the images of each fruit and vegetable. A: Bars represent average saturation of the insides and the geometrically matched areas of the skins of our fruits and vegetables, as represented in the CIELAB space (Chroma (C^*) divided by Lightness (L^*)). The error bars represent the standard error of the mean. B: Hue angle of the insides and the geometrically matched outsides of our fruits and vegetables, as represented in the CIELAB space (angle of each color about mid-gray when projected into the isoluminant plane). We find a significant correlation between the hue of the skin and inside, as indicated by the stars above the circular correlation value at the top of the graph. C: There is a significant correlation between the saturation of the insides and the geometrically matched areas of the skins of our fruit and vegetable objects, as indicated by the stars above the Pearson correlation value at the top of the graph.

on the skin; (2) the insides are not significantly less saturated than the skins; and (3) the mean hue angle of the color on the outside is predictive of the mean hue angle on the inside.

It is well established that different colorants are present in different fruits and vegetables [14–16]. Since the skin color could be used to predict the color of the inside, our results suggest that the colorants stay roughly the same. At the same time, their amount seems to vary throughout a fruit and vegetable. The insides of our objects were lighter than their skins, which is to say that more light was reflected from their insides. Since pigments absorb light, this indicates that there were a greater number of pigments present on the skin than on the inside and that the water on the insides could have made the surface more reflective.

B. Color Distributions on the Skins of Fruits and Vegetables and Chromatic Discrimination

In order to choose from a selection of objects, one must be able to discriminate between those objects in some manner. In the case of our fruits and vegetables, one could distinguish them by the colors on the surface, among other features. In fact, chromatic edges provide information for object segmentation in natural scenes, which is largely independent of the information provided by luminance edges [9]. Indeed, it has been hypothesized that one reason for the evolution of trichromatic color vision among Old World primates, as well as some female New World primates, was to better discriminate ripe from unripe fruit [40]. Here, we pursue the argument that our color vision system is closely tuned to the chromatic properties of our environment.

In previous work, Hansen *et al.* [41] measured discrimination performance for colored textures and natural objects. Observers were presented with either a chromatic noise pattern or an image of a fruit and vegetable, and the colors of the image were all shifted in the same color direction until the change was detectable to the observer. It was found that discrimination performance was worst when the colors of the image were shifted in the direction of elongation of the color distribution. The direction of elongation of the distribution can be assessed by representing it in the CIE xyY chromaticity diagram and fitting an ellipse to it, as shown in Fig. 8A. The major axis of the fitted ellipse will be the direction of elongation, provided that the distribution itself was not perfectly circular.

However, objects in the natural environment do not usually quickly change their color over short time spans, such as seconds. Rather, time-varying color signals are normally acquired by scanning one's eye across a scene. In that case, one might expect that our discrimination behavior has been somehow influenced by the natural distribution of colors in the environment. In particular, low-level color discrimination itself has been extensively studied. One of the earliest and most famous experiments on this topic was performed by MacAdam [17]. He presented one observer with a bipartite disk, similar to the color-matching stimulus that Maxwell [43] used. One-half of the disk was fixed in color, and the other half could be controlled by the observer. The color of the adjustable half was always anchored at the color of the fixed half, and the observer was provided with a knob that changed the chromaticity of the adjustable half in a direction radiating away from the

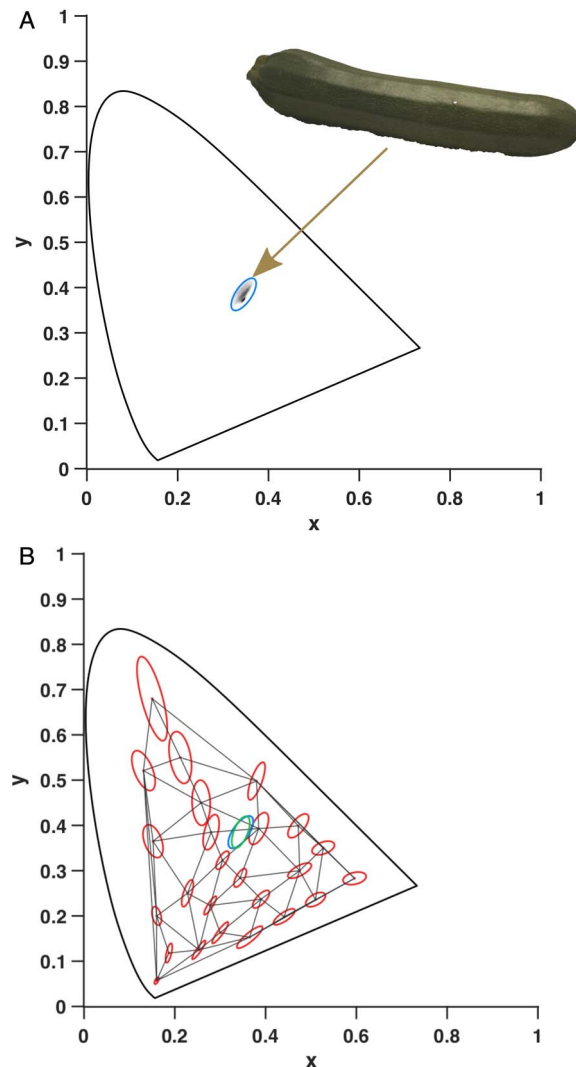


Fig. 8. Chromatic discrimination for natural objects and uniform colored patches. Panel A shows the chromaticity distribution of a zucchini (black cloud of points) in the CIE1931 xyY diagram. A blue ellipse has been fit to this distribution. Shifting all of the colors in the zucchini in the direction of the major axis of the fitted ellipse will be harder to detect than shifting all of the colors in the direction of the minor axis. Panel B shows the MacAdam ellipses in red. They have been scaled up by 10 \times for visibility purposes. The blue ellipse from panel A is also shown. The anchor points of the MacAdam ellipses have been connected in a Delaunay triangulation [42] to depict the process by which we interpolated the MacAdam ellipses, as described in the text. The green ellipse is an interpolated MacAdam ellipse whose anchor point is equivalent to the average chromaticity of the zucchini. One can see an almost perfect alignment between the orientation of the interpolated MacAdam ellipse and the ellipse that has been fit to the chromaticity distribution of the zucchini, indicating a potential connection between the colors of our natural environment and the discrimination behavior of our visual system.

anchoring chromaticity of the fixed half. The task of the observer was to change the adjustable half until both sides of the disk appeared equal.

If one measures the errors made for this task, in different directions emanating from the color of the fixed half of the disk,

then one finds that the errors form an ellipse around the anchoring chromaticity. It can be shown that the errors are $\sim 1/3$ times the size of a just noticeable difference in that region of color space, giving them the name, MacAdam discrimination ellipses. MacAdam measured 24 of these ellipses at different locations in the chromaticity diagram. In particular, the ellipses that are measured with this task exhibit different shapes and orientations at different locations in color space, showing that the CIE xyY chromaticity diagram is not perceptually uniform, although these differences were partially due to MacAdam not controlling for the observer's adaptation state [44]. Our goal was to test whether these differences correlate with the statistical properties of the colors of our natural samples, i.e., do the ellipses that were fit to the color distributions of the skins of our fruits and vegetables have similar orientations as the MacAdam ellipses? This would provide an indication that the visual system is tuned to its natural environment. In other words, we hypothesized that the visual system would benefit by discriminating a banana from a pear rather than discriminating the different shades of yellow within the surface of a banana.

Using the fitted ellipses discussed in "Finding the Orientation of the Fruit Distributions" in the "Methods" section, we went one by one through the 42 fruits and vegetables and found the three closest MacAdam ellipses that enclosed the center of the ellipse for the given fruit and vegetable by performing a lookup in a Delaunay triangulation [42] of all the MacAdam ellipse anchor points. We often needed to consider the enclosing MacAdam ellipses, because the average chromaticity of a random object is essentially never at the anchor point of any MacAdam ellipse. To rectify this problem, the anchoring points of the enclosing MacAdam ellipses were used as the vertices of a triangle. The barycentric coordinates of the average chromaticity for the given fruit and vegetable within this triangle were then used to linearly interpolate the parameters for the three enclosing MacAdam ellipses, giving an estimate of the MacAdam ellipse that one would have attained if one had measured it for the average chromaticity of the given fruit and vegetable. One can see the Delaunay triangulation, the (blue) ellipse fit to the color distribution of a zucchini, and the interpolated (green) MacAdam ellipse depicted in Fig. 8B. Note that in this plot, the MacAdam ellipses have been scaled up 10 \times from their original size for visibility purposes. If the center of a fruit and vegetable ellipse was located outside of the Delaunay triangulation, then a lookup in the triangulation was not successful. In that case, the closest MacAdam ellipse was chosen, using the distance between the center of the fruit and vegetable ellipse and the anchor point of the MacAdam ellipses. We checked to see how well the major axes of each fruit and vegetable ellipse aligned with those of the interpolated MacAdam ellipse. The orientation of each ellipse was chosen as the measure of interest, since the work of Hansen *et al.* [41], discussed above, showed that the elongation of the chromaticity distribution was the determining factor in discriminating it from a color-shifted version of itself.

Figure 9A depicts the distribution of the orientation of the ellipses fit to fruit and vegetable distributions and the orientation of the corresponding MacAdam ellipses. On average, the orientation difference was $30.98^\circ \pm 22.13^\circ$, with 24 fruits and vegetables (i.e., 57% of

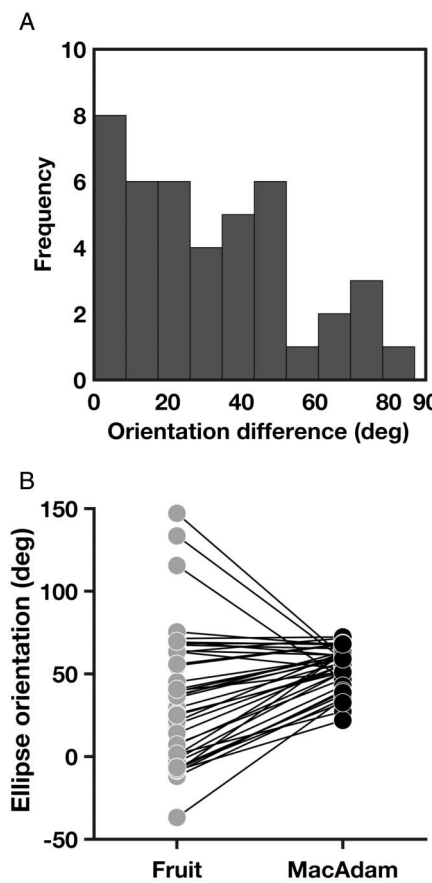


Fig. 9. Alignment of ellipses fit to fruit and vegetable distributions and interpolated MacAdam ellipses. A: Histogram of the differences in orientation between the major axis of the ellipse that was fit to the fruit and vegetable distribution and that of the respective interpolated MacAdam ellipse. B: Representation of the orientation of the ellipses fit to each fruit and vegetable chromaticity distribution (gray points) and the orientation of the MacAdam ellipses (black points). There was a significant circular correlation coefficient of 0.75.

the database) having orientation differences below 30.98° , indicating a good degree of alignment between the orientation of color distributions found on fruits and vegetables and the orientation of the MacAdam ellipses. In Fig. 9B, we compare the orientation of the ellipses fitted to the chromaticity distribution of the fruits and vegetables with the orientation of the MacAdam ellipses. If there is a relationship between the two quantities, then the orientation of the fruit and vegetable ellipses should correlate with the orientation of the corresponding MacAdam ellipses. Therefore, we computed a circular correlation coefficient between the two orientation variables, finding a 0.75 correlation coefficient ($z = 4.152$, $p < 0.001$). A non-parametric bootstrap analysis confirmed the result. We computed the confidence interval for the correlation coefficient under the null hypothesis that the orientations of the fitted ellipses and the interpolated MacAdam ellipses are not correlated. To do so, we randomly assigned each fitted ellipse to one of the interpolated ones (without replacement), and computed a new circular correlation coefficient. We determined the bootstrap-based 95% confidence interval, by repeating this

procedure 5000 times and computing the 0.025 and the 0.975 quantiles of the resulting distribution of correlation coefficients. The actual correlation we observed (0.75) is not included in the confidence interval ($[-0.3052\ 0.3031]$), allowing us to reject the null hypothesis. We take this to be evidence implying that the visual system is tuned to its environment, yet we want to be cautious not to make any claims about exact evolutionary processes.

4. DISCUSSION

We have managed to develop a publicly accessible hyperspectral database of fruits and vegetables, imaged under controlled lighting conditions, as well as an accompanying interface. The database itself, including the accompanying software, can be obtained at <http://www.allpsych.uni-giessen.de/GHIFVD>. We chose naturally occurring and biologically relevant surfaces, such as fruits and vegetables, to assess any possible relationships between the distributions of their colors and the properties of the human visual system. There is evidence suggesting that trichromacy evolved under the pressure of detecting edible targets against a foliage background [45] or to discern ripeness of fruits [40]; therefore the color of those natural surfaces is interesting for color vision research. The results of those studies were based on analyses of spectroradiometric measures of fruits and leaves in the diets of a number of primates. Because of the poor spatial resolution of the spectroradiometric measures, information about the color distributions of natural surfaces is largely lost, whereas hyperspectral images of fruits and vegetables allow analyses on full color distributions. In addition, the previous work on hyperspectral images used in color vision research were often of large-scale natural scenes [10,30,46], and much remains to be learned about the properties of the individual objects found in natural environments. Our analyses of the individual objects have led to intriguing results, such as the correlation between the orientation of the color distributions of our fruits and those of the MacAdam ellipses.

Our analysis revealed a correlation between the skin color and the inside of fruits and vegetables. It is well established that different colorants are present in different fruits and vegetables [14–16], but as far as we know, this is the first attempt to take hyperspectral images of both the skins and the insides of fruits and vegetables and to examine relationships between their colors, expanding on our knowledge of the colors in the natural world. Our results suggest that the colorants are roughly the same throughout a fruit and vegetable, but their concentration changes as one moves from the skin to the inside, since the skin color can be used to predict the color of the inside. The insides of our objects were lighter than their skins, which is to say that more light was reflected from their insides. Since pigments absorb light, this indicates that there were a greater number of pigments present on the skin than on the inside.

The analysis we performed on the color distributions of our fruits and vegetables shows that the orientation of the color distributions on their skins was close the orientations of the MacAdam ellipses. We speculate that our color vision is tuned to discriminate between different fruits and vegetables rather than discriminating the different hues within an object's surface. However, we do not make any strong claims about a direct

connection between the colors of fruits and vegetables and the color discrimination mechanisms of the human visual system. More work would be necessary to answer that question. Rather, we wanted to indicate an interesting correspondence that can have a behavioral relevance. The idea that color is useful for object discrimination is not new, however. For instance, Hansen and Gegenfurtner [9] computed the joint histograms of luminance and chromatic edges of a large set of calibrated natural images. Their results showed that chromatic edge contrast is an independent source of information for the segmentation of objects. Gegenfurtner and Rieger [47] employed a delayed match-to-sample task to test the role of color vision in the recognition of briefly presented images of natural scenes. For very brief presentations (16 ms), recognition was better for color images, even when they were tested in black and white. They argued that when the target is presented in color, but tested in black and white, color information could not be used in the decision; consequently, it was used during the encoding processes, such as edge detection, texture segmentation, or figure-ground segregation.

Our speculation that the perceptual representation of color is potentially tuned to the shape of the chromatic distribution of fruits and vegetables implies that color differences between natural objects are favored over the color differences within the surfaces of the objects themselves. In fact, the shape of MacAdam's results inspired many attempts to define a color space that is reasonably perceptually uniform (e.g., CIELAB, CIELUV) [25]. The idea that perceptual metrics are shaped by the surface properties of fruits might be at odds with a theory of a visual system optimized to accurately estimate the world's properties. However, Hoffman *et al.* [48] argued that the visual system does not need to accurately estimate the physical properties of the world, and strategies based on producing nonveridical estimates tuned to fitness could be beneficial at an evolutionary level. The idea we propose here is an example of perception potentially being tuned to a subset of the world's properties, at the expense of others.

Funding. Deutsche Forschungsgemeinschaft (DFG) (GE 879/9, SFB TRR 135 C2); Bundesministerium für Bildung und Forschung (BMBF); National Science Foundation (NSF) (01GQ1304).

Acknowledgment. The hyperspectral data are also freely available at <http://dx.doi.org/10.5281/zenodo.1186649>. We are thankful to the following for their helpful insight and assistance during the development of this project: Katja Doerschner, Marina Bloj, Matteo Valsecchi, Sergio Nascimento, Florian Bayer, Thorsten Hansen, Martin Giesel, David Weiß, and Romain Bachy.

REFERENCES

1. J. M. Watt and M. G. Breyer-Brandwijk, *The Medicinal and Poisonous Plants of Southern and Eastern Africa*, 2nd ed. (Livingstone, 1962).
2. F. Yasuma, T. Mitsunaga, D. Iso, and S. Nayar, "Generalized assorted pixel camera: postcapture control of resolution, dynamic range, and spectrum," *IEEE Trans. Image Process.* **19**, 2241–2253 (2010).
3. E. M. Valero, J. L. Nieves, S. M. C. Nascimento, K. Amano, and D. H. Foster, "Recovering spectral data from natural scenes with an RGB

- digital camera and colored filters," *Color Res. Appl.* **32**, 352–360 (2007).
4. D. H. Foster, K. Amano, and S. M. C. Nascimento, "Color constancy in natural scenes explained by global image statistics," *Visual Neurosci.* **23**, 341–349 (2006).
 5. C. Montagner, J. M. M. Linhares, M. Vilarigues, and S. M. C. Nascimento, "Statistics of colors in paintings and natural scenes," *J. Opt. Soc. Am. A* **33**, A170–A177 (2016).
 6. A. Chakrabarti and T. Zickler, "Statistics of real-world hyperspectral images," in *Proceedings of the IEEE Conference on Computer Vision and Pattern Recognition CVPR* (2011), pp. 193–200.
 7. C. A. Párraga, G. Brelstaff, T. Troscianko, and I. R. Moorehead, "Color and luminance information in natural scenes," *J. Opt. Soc. Am. A* **15**, 563–569 (1998).
 8. A. B. Poirson and B. A. Wandell, "Appearance of colored patterns: pattern–color separability," *J. Opt. Soc. Am. A* **10**, 2458–2470 (1993).
 9. T. Hansen and K. R. Gegenfurtner, "Independence of color and luminance edges in natural scenes," *Visual Neurosci.* **26**, 35–49 (2009).
 10. D. H. Foster, K. Amano, S. M. C. Nascimento, and M. J. Foster, "Frequency of metamerism in natural scenes," *J. Opt. Soc. Am. A* **23**, 2359–2372 (2006).
 11. T. Skauli and J. Farrell, "A collection of hyperspectral images for imaging systems research," *Proc. SPIE* **8660**, 86600C (2013).
 12. B. Arad and O. Ben-Shahar, "Sparse recovery of hyperspectral signal from natural RGB images," in *14th European Conference on Computer Vision, ECCV*, Vol. **9911** of Lecture Notes in Computer Science (Springer International, 2016), pp. 19–34.
 13. D. Wei, L. Zhang, D. Zhang, and Q. Pan, "Studies on hyperspectral face recognition in visible spectrum with feature band selection," *IEEE Trans. Syst. Man Cybern. A* **40**, 1354–1361 (2010).
 14. H.-E. Khoo, K. N. Prasad, K.-W. Kong, Y. Jiang, and A. Ismail, "Carotenoids and their isomers: color pigments in fruits and vegetables," *Molecules* **16**, 1710–1738 (2011).
 15. J. Gross, *Pigments in Vegetables: Chlorophylls and Carotenoids* (Van Nostrand Reinhold, 1991).
 16. J. E. Lancaster, C. E. Lister, P. F. Reay, and C. M. Triggs, "Influence of pigment composition on skin color in a wide range of fruit and vegetables," *J. Am. Soc. Hortic. Sci.* **122**, 594–598 (1997).
 17. D. L. MacAdam, "Visual sensitivities to color differences in daylight," *J. Opt. Soc. Am.* **32**, 247–274 (1942).
 18. N. D. Matsakis and F. S. Klock II, "The rust language," in *Proceedings of the ACM SIGAda Annual Conference on High Integrity Language Technology* (ACM, 2014), Vol. **34**, pp. 103–104.
 19. "The rust programming language," <https://www.rust-lang.org/>.
 20. Z. Xianyi, W. Qian, and Z. Yunquan, "Model-driven level 3 BLAS performance optimization on Loongson 3A processor," in *IEEE 18th International Conference on Parallel and Distributed Systems* (IEEE, 2012), pp. 684–691.
 21. Q. Wang, X. Zhang, Y. Zhang, and Q. Yi, "AUGEM: automatically generate high performance dense linear algebra kernels on x86 CPUs," in *Proceedings of the International Conference on High Performance Computing, Networking, Storage and Analysis* (ACM, 2013), pp. 1–12.
 22. K. Martinez and J. Cupitt, "VIPS: a highly tuned image processing software architecture," in *Proceedings of IEEE International Conference on Image Processing* (IEEE, 2005), pp. 574–577.
 23. "OpenCV," <https://opencv.org/>.
 24. C. Rother, V. Kolmogorov, A. Blake, C. Rother, V. Kolmogorov, and A. Blake, "GrabCut: interactive foreground extraction using iterated graph cuts," in *ACM Transactions on Graphics (TOG)* (2004), pp. 309–314.
 25. G. Wyszecki and W. S. Stiles, *Color Science: Concepts and Methods, Quantitative Data and Formulae* (Wiley, 1982).
 26. D. I. MacLeod and R. M. Boynton, "Chromaticity diagram showing cone excitation by stimuli of equal luminance," *J. Opt. Soc. Am.* **69**, 1183–1186 (1979).
 27. A. M. Derrington, J. Krauskopf, and P. Lennie, "Chromatic mechanisms in lateral geniculate nucleus of macaque," *J. Physiol.* **357**, 241–265 (1984).
 28. A. Stockman and L. T. Sharpe, "The spectral sensitivities of the middle- and long-wavelength-sensitive cones derived from measurements in observers of known genotype," *Vis. Res.* **40**, 1711–1737 (2000).
 29. A. Stockman, L. T. Sharpe, and C. Fach, "The spectral sensitivity of the human short-wavelength sensitive cones derived from thresholds and color matches," *Vis. Res.* **39**, 2901–2927 (1999).
 30. S. M. C. Nascimento, D. H. Foster, and K. Amano, "Psychophysical estimates of the number of spectral-reflectance basis functions needed to reproduce natural scenes," *J. Opt. Soc. Am. A* **22**, 1017–1022 (2005).
 31. M. D. Fairchild, *Color Appearance Models*, 3rd ed. (Wiley, 2013).
 32. F. Schiller and K. R. Gegenfurtner, "Perception of saturation in natural scenes," *J. Opt. Soc. Am. A* **33**, A194–A206 (2016).
 33. F. Schiller, M. Valsecchi, and K. R. Gegenfurtner, "An evaluation of different measures of color saturation," *Vis. Res.* (to be published), doi: [10.1016/j.visres.2017.04.012](https://doi.org/10.1016/j.visres.2017.04.012).
 34. S. M. C. Nascimento, J. M. M. Linhares, C. Montagner, C. A. R. João, K. Amano, C. Alfaro, and A. Bailão, "The colors of paintings and viewers' preferences," *Vis. Res.* **130**, 76–84 (2017).
 35. C. Montagner, J. M. M. Linhares, M. Vilarigues, M. J. Melo, and S. M. C. Nascimento, "Supporting history of art with colorimetry: the paintings of Amadeo de Souza-Cardoso," *Color Res. Appl.* **7**, 3 (2017).
 36. D. Lee, *Nature's Palette* (University of Chicago, 2007).
 37. S. R. Jammalamadaka and Y. R. Sarma, "A correlation coefficient for angular variables," in *Statistical Theory and Data Analysis II*, K. Matusita, ed. (1988), pp. 349–364.
 38. S. R. Jammalamadaka and A. SenGupta, *Topics in Circular Statistics* (World Scientific, 2001).
 39. P. Berens, "CircStat: a MATLAB toolbox for circular statistics," *J. Statist. Softw.* **31**, 1–21 (2009).
 40. P. Sumner and J. D. Mollon, "Chromaticity as a signal of ripeness in fruits taken by primates," *J. Exp. Biol.* **203**, 1987–2000 (2000).
 41. T. Hansen, M. Giesel, and K. R. Gegenfurtner, "Chromatic discrimination of natural objects," *J. Vis.* **8**(1):2, 1–19 (2008).
 42. B. N. Delaunay, "Sur le sphère vide," *Bull. Acad. Sci. USSR* **6**, 793–800 (1934).
 43. J. C. Maxwell, "XVIII—Experiments on colour, as perceived by the eye, with remarks on colour-blindness," *Trans. R. Soc. Edinburgh* **21**, 275–298 (1857).
 44. J. Krauskopf and K. Gegenfurtner, "Color discrimination and adaptation," *Vis. Res.* **32**, 2165–2175 (1992).
 45. P. Sumner and J. D. Mollon, "Catarrhine photopigments are optimized for detecting targets against a foliage background," *J. Exp. Biol.* **203**, 1963–1986 (2000).
 46. D. H. Foster and S. M. C. Nascimento, "Relational colour constancy from invariant cone-excitation ratios," *Proc. R. Soc. B* **257**, 115–121 (1994).
 47. K. R. Gegenfurtner and J. Rieger, "Sensory and cognitive contributions of color to the recognition of natural scenes," *Curr. Biol.* **10**, 805–808 (2000).
 48. D. D. Hoffman, M. Singh, and C. Prakash, "The interface theory of perception," *Psychon. Bull. Rev.* **22**, 1480–1506 (2015).